A Rule-Based Approach for Interpretable Intensity-Modulated Radiation Therapy Treatment Selection

Anonymous Authors

Knowledge-Based Planning (KBP) for Intensity-modulated radiation therapy (IMRT) is a data-driven approach that utilises real-time medical imaging to adjust the radiation dose as needed. This is important because tumours can move and change shape during treatment, so a standard plan may not be accurate.

This study presents an interpretable Artificial Intelligence (AI) model intended to decide between several IMRT treatment alternatives and determining which one is the best. To this endeavor, the development of an Adaptive Neuforuzzy Adaptive Inference System (ANFIS) is proposed, which combines the potential of a neural network with the interpretability of a decision making system that makes use of natural language.

The training of the model it's being conducted in a supervised manner using the OpenKBP challenge data repository. In addition we have developed a data augmentation method that is supported by Diffusion Probabilistic Models (DPMs). This approach enables the generation of a wider spectrum of treatment qualities, including low quality plans.

The primary advantage of this framework resides in its ability to offer explanations, thereby facilitating a rapid and straightforward assessment of treatments by healthcare professionals. Moreover, it serves as a valuable means to test hypotheses concerning the quality of IMRT treatments. The achieved outcomes reveal a promising future for the developed tool, indicating that it holds substantial potential to establish itself as a reference in the realm of explainable IMRT treatment selection tools.

***Index Terms*—Knowledge Based Planning, Artificial Intelligence, Fuzzy Inference Systems**

I. Introduction

In recent decades, significant advancements have been made in the field of radiotherapy. Among these advances, healthcare organisations are exploring AI-based solutions to improve the accuracy and efficacy of treatments. Indeed, numerous studies have shown that AI techniques enable more personalised treatments to be offered to cancer patients [1], [2]. One emerging discipline within radiotherapy planning is knowledge-based planning (KBP) [3], which involves using data-based models to determine the optimal radiation doses for each treatment based on computed tomography (CT) scans and clinical data. Currently, deep learning models have established as leaders in terms of both speed and accuracy in this domain [4].

While conventional KBP systems strive to identify a single, optimal treatment, there are external factors that can influence treatment efficacy, making diverse treatment options valuable for expert decision-making. The advent of Generative AI (GAI) has pushed KBP research forward, and studies like Barbier et al. [4] have demonstrated the potential of GAI models in this domain. GAI models possess the ability to generate treatment variations from a single input. However, this capability introduces a new challenge in KBP, which is to effectively select the most suitable treatment variant among the generated options.

The selection between different treatments has still not been extensively studied. In fact, treatment selection in radiotherapy requires the fulfilment of a comprehensive set of regulations and conditions, which can be transformed into a multiple linear optimisation problem. In numerous instances, it becomes impossible to satisfy all constraints, forcing doctors to rely on their observations of patient CT scans and dose distributions to make decisions. Additionally, there are situations where, despite meeting all the restrictions, a better treatment option may still exist.

This study aims to develop a novel KBP model that goes beyond generating radiotherapy treatments and delves into determining which treatments are the best ones, establishing an order among them. Additionally, we aim to interpret the rationale behind the model's evaluation of each treatment's quality. The framework is composed of two AI models: a set of image to image Diffusion Probabilistic Models (DPMs) which serves as a generator of different quality treatments, and a modified version of an Adaptive Neurofuzzy Inference System (ANFIS) that determines the best treatment option and identifies the factors contributing to optimal outcomes. To accomplish this, we have conducted an experimentation on the data provided in the OpenKBP Challenge.

The paper proceeds as follows: Section II establishes the theoretical foundations of radiotherapy, deep learning and fuzzy inference systems which are essential for comprehending the subsequent sections. The third section (III) provides detailed descriptions of the dataset and methodologies employed in the research. Subsequently, section IV focuses on the experimentation and results. Finally, in section V the conclusions and future work are summarised.

II. Background

Radiotherapy is a medical treatment used to fight the cancer by delivering high-energy radiation into the tumour environment [5]. In this section we review the mechanism that makes this treatment effective and which AI techniques have been shown to be successful in KBP for IMRT.

A. Clinical Background

The role of radiation is to break down the DNA helices of cancer cells, provoking them to stop dividing and inducing them to apoptosis (cell death) [6]. However, radiation particles can damage other cells and proteins and there is no mechanism to isolate tumour cells. Hence, the goal of radiotherapy is to

deliver a high dose of radiation to the tumour while minimising the exposure of healthy tissue to radiation.

In this research we address Intensity-modulated radiation therapy (IMRT) treatments, due to the fact that they are commonly used for KBP systems [7]. IMRT employs specialised medical imaging software and linear accelerators to deliver precise treatment while minimising radiation exposure to surrounding tissues. This is achieved through the strategic positioning of radiation beams, which emit varying intensities tailored to conform to the tumour's shape. Planning IMRT treatments involves a personalised process coordinated by a team of radiation oncologists, medical physicists, and dosimetrists. With this in mind, we outline the three key stages of IMRT.

- Firstly main target tumour volumes are contoured. According to the OpenKBP dataset Section III, we exclusively examine the Planning Target Volume (PTV), a precise representation of the tumour volume augmented with a margin of safety to ensure complete tumour eradication and minimise the possibility of residual cancer cells [8]. The Organs At Risk (OARs) in the area around the tumour are also contoured [9]. The OARs are particularly important for dosimetry, since, once the treatment is completed, the radiation absorbed by the OARs can be measured [10].
- The second stage of the process focuses on optimising the dose distribution. The KBP systems are built around the method of inverse optimisation [11]. This method involves the assignment of a target dose distribution, followed by the determination of the optimal placement of the radiation beams to achieve the desired distribution.
- Finally, the most suitable treatment is selected by considering both qualitative information (visual assessment of the treatment plan images) and quantitative information (calculation of dose metrics). Quantitative information is essential because it allows us to verify whether the treatment complies with certain dose restrictions in the form of a linear programming problem.

IMRT planning in most cases is performed only once for each treatment despite the fact that the tumour morphology evolves continuously. Therefore, KBP models allow for a continuous review of the patient, promoting *Adaptive Radiotherapy* [12].

B. Artificial Intelligence Background

According to Ge et al. [3], there are two main approaches to KBP models for IMRT. The first approach, known as "Case and Atlas-based methods," uses similarity measures to compare a given treatment with previously stored high-quality treatments in databases [13], [14]. After that, the most similar treatments are selected, and positive aspects from these are transferred to refine the current treatment. Case and Atlas-based methods represent approximately the 30% of the articles evaluated [3].

The second approach involves machine learning and statistical models, where classical regression techniques and support vector machines are predominant [15]. However, due to the rise of deep learning, the state of the art in the KBP area has shifted towards new artificial neural network models. [16].

In particular, in order to address the need for diverse treatment plans, we decided to focus the research on generative artificial intelligence (GAI) models. As discussed in the introduction, knowledge-based IMRT planning systems have successfully employed generative models like Generative Adversarial Networks [4].

Recently, diffusion probabilistic models (DPMs) have emerged within the GAI domain, showcasing remarkable performance in image-to-image tasks [17]. In fact, the MedSegDiff DPM model [18] stands out for its innovative approach to conditioning diffusion models for medical image segmentation tasks. Diffusion Probabilistic Models (DPMs) introduce Gaussian random noise into model inputs progressively during training. This forces the deep learning model to learn to reconstruct the original information from the corrupted data. In image-to-image tasks, a U-Net architecture is commonly employed as the denoising model [19]. During inference, the model receives a random Gaussian noise input and produces an output that adheres to the provided conditioning information. This conditioning mechanism is a key feature of DPMs, allowing users to incorporate additional information, typically through text or image prompts, to guide the model's output.

In the KBP-IMRT scenario, the conditioning mechanism is provided by the patient's CT scan and the volumes of interest (PTVs and OARs). By this way, the model aims to accurately estimate the radiation dose distribution based on random Gaussian noise, essentially a pixel-wise regression task with 2D-3D images.

Regarding the loss function, the same philosophy as in the variational auto-encoder is followed [20]. In short, starting from the negative log-likelihood function and making use of the Kullback–Leibler divergence measure [21], it can be deduced that the negative log-likelihood it is equivalent to calculate:

$$l_1 = ||\epsilon_t - \epsilon_\theta(\vec{z}_t, t, \tau)||_2^2 \tag{1}$$

which is the difference between the theoretical noise to be removed at time step t, ϵ_t, the prediction given by the model ϵ_θ, which depends on the noisy image at time step t, $\vec{z}_t$, and the conditioning information, τ. The elaboration of this result can be found at *"Denoising Diffusion Probabilistic Models"* [22].

It is important to note that all of the above models are black box models. In healthcare applications, the reliability of deep learning methodologies is a critical concern. While accuracy is often emphasised, it's equally important to understand the reasoning behind the artificial network's decisions. This is where Explainable Artificial Intelligence (XAI) comes in, a field dedicated to understanding the decision-making process within AI systems [23].

Fuzzy logic, in particular, holds promise in XAI due to its ability to capture human-like reasoning. Human reasoning often follows the "IF antecedent THEN consequent" structure, which can be effectively modelled using fuzzy rules [24]. Antecedents represent linguistic premises expressed as fuzzy variables, while consequents represent the conclusions extracted from evaluating these premises. Consequents can take various forms, including constants, real values, classes, or even fuzzy sets.

A fuzzy rule system consists of a collection of fuzzy rules that govern the behaviour of a system based on input data. Its inference process entails evaluating input values against all rules and then making a collective decision to determine the system's response to the input. In this work we propose to use Takagi-Sugeno-Kang inference system, commonly known as as TSK, where the consequents of each rule are real values [25].

TSK can be effectively implemented and optimised using a neural network called Adaptive Neuro-Fuzzy Inference System (ANFIS) [26]. This hybrid system combines the gradient-based optimisation with the fuzzy logic framework to model complex systems. In Section III-C we detail the implementation of the ANFIS model its interpretability is discussed in Section IV-A.

III. Methodology

The methodology for this paper is outlined below. As in any supervised learning problem, data play a vital role.

A. Data

The Open Knowledge-Based Planning Challenge (OpenKBP) [27] was launched in 2020 with the aim of taking a step forward in IMRT-KBP frameworks and due to the difficulty of finding open source data on this topic. To this end, the American Association of Physicists in Medicine developed a dataset by cleaning and processing CT images of The Cancer Imaging Archive open database. In particular, public CT scans were taken and processed from 340 patients who underwent radiotherapy treatments of neck or head cancer. These set of patients were divided into three categories: 200 patients for training, 40 for model validation and the rest (100) for evaluation. The evaluation (test) data was not provided to the challenge participants and it was used to evaluate the assessment metrics. In this work, we intend to use identical divisions as the ones initially established. This choice allow us to conveniently compare outcomes with other teams of the challenge without worrying about biased partitions.

The challenge was evaluated through two metrics related only to dose distribution. The participants worked with both CT images and target contours (PTVs + OARs).

The first metric is known as the Dose Score (DS), that is the Mean Absolute Error (MAE) between the real plan and the predicted one.

The second metric is the Dose Volume Histogram Score (DVHS). For the OARs, two criteria are taken into account: the mean radiation dose received by an OAR, D_{mean}, and the maximum dose applied to 0.1 cubic centimetre's of the tissue, $D_{0.1cc}$. Additionally, there exist three tumour target criteria, namely D_{01}, D_{95}, and D_{99}, which correspond to the radiation doses received by the top 1% (99th percentile), 95% and 99% of voxels within target. Once again, the DVHS is the MAE between the real measure and the predicted one.

B. Generation of synthetic plans

Despite the amount of data structures provided by this dataset, we aim to determine the quality of a treatment. To do this in a supervised manner, we need to obtain a set of examples with different qualities. It can be assumed that the dataset's samples are of good quality since they have been used in real case scenarios. However, we lack data representing a range of treatment qualities.

To address this issue, we propose generating synthetic treatments using an intelligent data augmentation technique. This technique employs multiple DPMs to generate a large number of treatments from a single input.

Inspired by MedSegDiff [18], our proposed DPM design aims to adapt this approach to the complexities of IMRT, which demands modifications to handle pixel-wise regression. The DPM is formed by two U-Nets, each serving a distinct purpose. The first U-Net, the Denoising U-Net (DUNet), is tasked with reducing Gaussian noise from the input image. In order to determine the quantity of noise to be reduced, it integrates temporal information encoded as temporal sinusoidal embeddings. In addition, the conditioning mechanism provides insight into what characteristics the denoised output should have. As a result, the output of the denoising U-Net represents the amount of noise to be eliminated, in terms of mean and variance. This noise is then subtracted from the input image, yielding a denoised representation. This process is cyclical, with the output becoming the input for the model at the subsequent timestamp until reaching the initial time step.

The second UNet, the Conditioning UNet (CUNet), is responsible of predicting the dossimetry based on the CT scan and structure masks, including organs at risk (OARs) and planning target volumes (PTVs). In essence, the CUNet's primary objective matches that of the overall diffusion model. By this way, the CUNet's decoder features acquire knowledge pertinent to the treatment planning process. These features can then be employed as conditioning information by integrating them with the DUNet's encoder. This merging mechanism, termed anchor conditioning by the authors [18]. The model prediction is the combination of the individual predictions of the DUNet and CUNet, respectively $\mathbf{y}^D$ and $\mathbf{y}^C$:

$$\hat{\mathbf{y}} = \omega \cdot \mathbf{y}^D + (1 - \omega) \cdot \mathbf{y}^C \tag{2}$$

here we include ω as the chaos parameter. The higher the parameter, the more important the DUNet becomes in the prediction and therefore, the more variability it will have. Figure 1 shows the overall architecture of the proposed DPM.

Even though a single DPM model can generate different treatments, we wanted to take advantage of the fact that the problem we address is multi-objective, meaning that the model's objective function consists of several factors. These objectives include the CUNet loss function, the DUNet loss function (Eq. 1), minimising dose to OARs and maximising dose to PTVs. Let us now consider the mean value within the PTV targets as $\hat{d}$, the mean dose value of the OARs as $\bar{d}$, the ground truth as $\mathbf{y}$ and any arbitrary parameters p_1, p_2. Thus, keeping in mind the DS and DVHS, we can define the loss function of the CUNet as follows:

$$l_2 = MAE(\mathbf{y}, \hat{\mathbf{y}}^{\mathbf{C}}) + \frac{p_1}{\hat{d}} + \frac{\bar{d}}{p_2}. \tag{3}$$

Consequently, the overall loss function is computed as:

$$l = p_3 \cdot l_1 + (1 - p_3) \cdot l_2. \tag{4}$$

Here, we introduce p_3 as the parameter that quantifies the influence of the DUNet model over the CUNet.

We propose to train multiple DPMs in which each factor of the objective function, p_1, p_2, p_3, is modified. This approach yield specialist generative models biased towards certain factors. For instance, one model may tend to be more aggressive and administer slightly higher doses, while another may be more conservative and strive to minimise the dose absorbed by the risk organs.

This technique prevents the model from replicating the behaviour of the training data, while simultaneously generating treatments that could be real. Furthermore, we can assess the quality of each prediction based on the assumption that the treatments with the highest quality are the real ones. The quality of each prediction then, is determined by its dissimilarity to its reference treatment. Specifically, we have selected the MAE due to its suitability for the OpenKBP Challenge.

C. Treatment Selection

As a decision-making system aiming to replicate the reasoning of oncologists, it is essential to establish the fuzzy variables that will be integrated into the rule system. We have opted to focus on those evaluated in the OpenKBP challenge. Variables such as D_{mean} and $D_{0.1cc}$ are considered for OARs, as well as D_{01} and D_{95} for PTVs. It is important to recall that missing values are not taken into account.

Another important decision in the development of the Fuzzy System involves defining the number of fuzzy sets associated with each fuzzy variable. To enhance simplicity and interpretability of the system, each fuzzy variable consist of three fuzzy sets: "LOW", "MEDIUM", and "HIGH". These fuzzy sets follow a Gaussian distribution as stated in Eq. 5. In order to help the optimisation procedure and align it with the objective of maximising interpretability, we propose a fixed initialisation approach with a small learning rate for the parameters of the fuzzy sets. This methodology should avoid scenarios where the model evolves towards a solution in which there is no relation between the semantics of the linguistic label and the shape of the fuzzy set.

The rules have been established by a team of oncologists and physicists from the Public Hospital of Navarre. Table I presents the set of ten rules that aim to explain the factors determining the quality of a treatment. While there could be numerous additional rules, an interpretable model should strive for simplicity. It is important to note that each rule in Table I provides a label indication of the expected quality when activated.

However, in the ANFIS model, the outputs are going to be given as numerical values rather than labels. The consequent represents the measure of quality assigned to the input treatment. In this context, we are only concerned with establishing a ranking among the treatments, so numerical values do not hold inherent meaning. The interpretability of the system lies in understanding which rules are activated and why, rather than interpreting the numerical values themselves.

Regarding implementation, we have decided to modify the ANFIS architecture to overcome the limitations imposed by the ANFIS baseline model's aggregations. The proposed ANFIS is divided into five layers and each one computes a specific stage of the TSK model. Considering a vector $\vec{x} \in \mathbb{R}^n$ a system composed of k rules, $i \in \{1, \ldots, n\}$ and $j \in \{1, \ldots, k\}$ the forward process proceeds as follows:

1) The first layer is known as membership layer and extracts the membership values of the input data for each rule. It is common to use Gaussian fuzzy sets:

$$A_{ij}(x) = e^{-(\frac{x_i - \mu_{ij}}{\sigma_{ij}}^2)}. \tag{5}$$

   Here, μ_{ij} and σ_{ij} are parameters of the network.
2) The second layer computes the firing strength of each rule, generally using the product or minimum operator. However the use of a product to determine the firing strength of a rule implies that a single membership degree with a low value inhibits the rule activation. To address this issue, we propose using a averaging aggregation scheme:

$$w_j = \begin{cases} \frac{1}{n}\sum_{i=0}^{n} x_i, & \text{if } \min(\vec{x}) \geq a \\ \prod_{i=0}^{n} x_i, & \text{otherwise} \end{cases}, \tag{6}$$

   where a is a threshold determined by the user.
3) The third layer normalises the firing strengths from the previous layer.
4) In the fourth layer, the consequent of each rule is calculated by a linear function. Here, we propose to extend the TSK model to allow for nonlinear consequent functions, reducing the need for an excessive number of rules to represent complex nonlinear relationships:

$$f_j(\vec{x}) = \varphi(\sum_{i=1}^{n}(\alpha_{ij} \cdot x_i) + b_j). \tag{7}$$

   Once again, $\vec{\alpha}_j = (\alpha_{1j}, \ldots, \alpha_{nj})$ and b_j are parameters of the network and φ is a non linear activation function.

5) The final layer, known as defuzzification layer, collects the consequent and firing strength of each rule to return the crisp output value, typically using a defuzzification method such as the centroid:

$$y = \frac{\sum_{j=1}^{k} w_j g_j(\vec{x})}{\sum_{j=1}^{k} w_j}. \quad (8)$$

We explore in Section IV-A how these modifications improve the ANFIS model's flexibility and adaptability to the proposed scenario.

IV. Experimentation

A. Results

A personal computer with an AMD RX 6800XT GPU has been used to train the data augmentation models. The use of AMD graphics cards today is possible thanks to the ROCm ecosystem, which currently supports Pytorch and simulates CUDA functionality [28]. The size of the DPM is about 26 million parameters, which is on par with pytorch's ResNet50 model [29]. For a DPM model this is a small number of parameters, however, due to the resource capacity and our goal of handling treatments of varying qualities, it is an affordable size. The training process required about 400,000 iterations (backward steps) for each DPM and during inference we have incorporated the DPM++ solver [30], which solves stochastic ordinary differential equations to perform the inference process within 15-30 steps, reducing significantly the overall computational cost. Figure 2 showcases an example of how our models perform inference with the DPM++ solver.

We developed four DPM with distinct characteristics. The primary model, denoted as $Balanced$, serves as the reference model and has been trained using Eq. 4 under the parameters $p_1 = 60$, $p_2 = 30$, and $p_3 = 0.5$. Following this, a model named $Biased$ was trained, prioritising DUNet over CUNet (by increasing p_3). Additionally, we conducted finetuning on the $Balanced$ model, resulting in two versions: $Aggressive$, which tends to administer higher doses (by increasing p_1), and $Conservative$, which generally maintains lower doses (by increasing p_2).

Results over the evaluation data are presented in Table II. While those results are not comparable to the OpenKBP benchmark values (see [27]), are in line with our goal of broadening the spectrum of treatment qualities. As illustrated in Figure 4, this extension was successfully achieved, although the ideal distribution would be an uniform distribution in order to inhibit any unbalanced data issues. Recall that we are measuring dissimilarity between the original and predicted treatment and therefore the lower the score, the higher the quality.

From a qualitative perspective, we observed that the dosimetries are quite close to the real dosimetry, especially in the case of the conservative and aggressive model. Figure 3 shows a randomly selected patient in the evaluation set predicted by the four DPMs. However, the models tend to underestimate the highest doses consistently. It is crucial to emphasise the importance of realistic treatment plans. In fact, this illustration serves as a prime example, where the model predicts zero dose for the spinal cord (an empty dot into the middle), which is unrealistic as it is not possible to position the beams to avoid the spinal cord while irradiating the surrounding areas. For this reason, the DVHS is almost as important as the DS.

In order to evaluate the quality prediction performance in ANFIS, we trained it on a synthetic dataset comprising five samples for each level of chaos and model variant. This resulted in a total of 4.400 synthetic treatments, from which we extracted the metrics of interest. After training the ANFIS model with five different initialisation, we obtained results that suggest an average error of 1.5 points when predicting the quality of a treatment as stated in table III. In addition, we observe how the proposed modification in the firing strength (Eq. 6) affects the model performance. More precisely, by setting a threshold $a = 0.1$, we successfully address the inhibition of rule activation due to a single small value. The differences are insignificant for the changes in the consequent.

To address treatment selection performance, we propose to leverage ANFIS as an ensemble and integrate it with DPMs to form a complete KBP system. The proposed experimental framework is illustrated in Figure 7. Beginning with CT scans containing segmented OARs and PTVs (Step 1), multiple plans are computed for each DPM model (Steps 2 to 4). Following this, the outcomes of both the DUNet and the CUNet are combined (Step 5). Lastly, ANFIS identifies the most appropriate treatment and offers valuable insights into the key rules that played a role in the treatment selection process (Step 6). The experimentation is concluded by running it with the complete pipeline, yielding a DS of **5.493** and a DVHS of **5.267** during evaluation data. These outcomes stand in direct competition with the $Conservative$ model (Table II).

B. Interpretability

Finally, we demonstrate through an illustrative example how ANFIS provides an interpretation that clarifies why a particular treatment is considered the most optimal.

In Figure 5, we can discern the activation of specific rules, revealing a correlation with the treatment types outlined by experts in Table I. For instance, in the context of "decent treatment," rule eight exhibits the highest activation, aligning with expert opinions associating it with effective treatment. Conversely, in the case of "bad treatment," the predominant activation is observed in the third rule, consistent with expert assertions that rule three signifies suboptimal treatment. The importance of each rule, represented by colour in Figure 5, is a parameter introduced in the network to prioritise crucial rules, recognising that not all rules carry equal importance.

Delving deeper, we seek to identify the factors or premises triggering these activations. As depicted in Figure 6, a heatmap illustrates fuzzy memberships, offering insights into the factors influencing the treatment evaluation. Experts might attribute the classification of a treatment as decent to low doses administered to the parotid and esophagus, coupled with a

high dose to the PTV. However, the treatment is not flawless, with an activation score of 0.4, indicating the presence of premises that deviate from the truth with a considerable degree of membership.

V. Conclusion

Media página

Acknowledgment

The authors would like to thank...

References

[1] S. Siddique and J. C. Chow, "Artificial intelligence in radiotherapy," *Reports of Practical Oncology and Radiotherapy*, vol. 25, no. 4, pp. 656–666, 2020.

[2] J. C. L. Chow, "Artificial intelligence in radiotherapy and patient care," in *Artificial Intelligence in Medicine*. Springer, 2021, pp. 1–13.

[3] Y. Ge and Q. J. Wu, "Knowledge-based planning for intensity-modulated radiation therapy: a review of data-driven approaches," *Medical physics*, vol. 46, no. 6, pp. 2760–2775, 2019.

[4] A. Babier, R. Mahmood, A. L. McNiven, A. Diamant, and T. C. Chan, "Knowledge-based automated planning with three-dimensional generative adversarial networks," *Medical Physics*, vol. 47, no. 2, pp. 297–306, 2020.

[5] F. M. Khan and J. P. Gibbons, *Khan's the physics of radiation therapy*. Lippincott Williams & Wilkins, 2014.

[6] M. Garcia-Barros, F. Paris, C. Cordon-Cardo, D. Lyden, S. Rafii, A. Haimovitz-Friedman, Z. Fuks, and R. Kolesnick, "Tumor response to radiotherapy regulated by endothelial cell apoptosis," *Science*, vol. 300, no. 5622, pp. 1155–1159, 2003.

[7] B. S. Teh, S. Y. Woo, and E. B. Butler, "Intensity modulated radiation therapy (imrt): a new promising technology in radiation oncology," *The oncologist*, vol. 4, no. 6, pp. 433–442, 1999.

[8] J. A. Antolak and I. I. Rosen, "Planning target volumes for radiotherapy: how much margin is needed?" *International Journal of Radiation Oncology* Biology* Physics*, vol. 44, no. 5, pp. 1165–1170, 1999.

[9] M. E. Christianen, J. A. Langendijk, H. E. Westerlaan, T. A. van de Water, and H. P. Bijl, "Delineation of organs at risk involved in swallowing for radiotherapy treatment planning," *Radiotherapy and Oncology*, vol. 101, no. 3, pp. 394–402, 2011.

[10] G. Noël and D. Antoni, "Organs at risk radiation dose constraints," *Cancer/Radiothérapie*, vol. 26, no. 1-2, pp. 59–75, 2022.

[11] A. Babier, J. J. Boutilier, M. B. Sharpe, A. L. McNiven, and T. C. Chan, "Inverse optimization of objective function weights for treatment planning using clinical dose-volume histograms," *Physics in Medicine & Biology*, vol. 63, no. 10, p. 105004, 2018.

[12] D. Yan, F. Vicini, J. Wong, and A. Martinez, "Adaptive radiation therapy," *Physics in Medicine & Biology*, vol. 42, no. 1, p. 123, 1997.

[13] V. Chanyavanich, S. K. Das, W. R. Lee, and J. Y. Lo, "Knowledge-based imrt treatment planning for prostate cancer," *Medical physics*, vol. 38, no. 5, pp. 2515–2522, 2011.

[14] N. Mishra, S. Petrovic, and S. Sundar, "A self-adaptive case-based reasoning system for dose planning in prostate cancer radiotherapy," *Medical physics*, vol. 38, no. 12, pp. 6528–6538, 2011.

[15] W. E. Brown, K. Sung, D. M. Aleman, E. Moreno-Centeno, T. G. Purdie, and C. J. McIntosh, "Guided undersampling classification for automated radiation therapy quality assurance of prostate cancer treatment," *Medical physics*, vol. 45, no. 4, pp. 1306–1316, 2018.

[16] C. Wang, X. Zhu, J. C. Hong, and D. Zheng, "Artificial intelligence in radiotherapy treatment planning: present and future," *Technology in cancer research & treatment*, vol. 18, p. 1533033819873922, 2019.

[17] R. Rombach, A. Blattmann, D. Lorenz, P. Esser, and B. Ommer, "High-resolution image synthesis with latent diffusion models," in *Proceedings of the IEEE/CVF conference on computer vision and pattern recognition*, 2022, pp. 10 684–10 695.

[18] J. Wu, R. Fu, H. Fang, Y. Zhang, and Y. Xu, "Medsegdiff-v2: Diffusion based medical image segmentation with transformer," *arXiv preprint arXiv:2301.11798*, 2023.

[19] O. Ronneberger, P. Fischer, and T. Brox, "U-net: Convolutional networks for biomedical image segmentation," in *Medical Image Computing and Computer-Assisted Intervention–MICCAI 2015: 18th International Conference, Munich, Germany, October 5-9, 2015, Proceedings, Part III 18*. Springer, 2015, pp. 234–241.

[20] D. P. Kingma, M. Welling *et al.*, "An introduction to variational autoencoders," *Foundations and Trends® in Machine Learning*, vol. 12, no. 4, pp. 307–392, 2019.

[21] T. Van Erven and P. Harremos, "Rényi divergence and kullback-leibler divergence," *IEEE Transactions on Information Theory*, vol. 60, no. 7, pp. 3797–3820, 2014.

[22] J. Ho, A. Jain, and P. Abbeel, "Denoising diffusion probabilistic models," *Advances in Neural Information Processing Systems*, vol. 33, pp. 6840–6851, 2020.

[23] V. Petrauskas, G. Damuleviciene, A. Dobrovolskis, J. Dovydaitis, A. Janaviciute, R. Jasinevicius, E. Kazanavicius, J. Knasiene, V. Lesauskaite, A. Liutkevicius *et al.*, "Xai-based medical decision support system model," *Int. J. Sci. Res. Publ*, vol. 10, no. 12, pp. 598–607, 2020.

[24] H. Hagras, "Toward human-understandable, explainable ai," *Computer*, vol. 51, no. 9, pp. 28–36, 2018.

[25] T. Takagi and M. Sugeno, "Fuzzy identification of systems and its applications to modeling and control," *IEEE transactions on systems, man, and cybernetics*, no. 1, pp. 116–132, 1985.

[26] J.-S. Jang, "Anfis: adaptive-network-based fuzzy inference system," *IEEE transactions on systems, man, and cybernetics*, vol. 23, no. 3, pp. 665–685, 1993.

[27] A. Babier, B. Zhang, R. Mahmood, K. L. Moore, T. G. Purdie, A. L. McNiven, and T. C. Y. Chan, "OpenKBP: The open-access knowledge-based planning grand challenge and dataset," *Medical Physics*, vol. 48, no. 9, pp. 5549–5561, jun 2021. [Online]. Available: https://doi.org/10.1002%2Fmp.14845

[28] N. Otterness and J. H. Anderson, "Amd gpus as an alternative to nvidia for supporting real-time workloads," in *32nd Euromicro conference on real-time systems (ECRTS 2020)*. Schloss Dagstuhl-Leibniz-Zentrum für Informatik, 2020.

[29] S. Mascarenhas and M. Agarwal, "A comparison between vgg16, vgg19 and resnet50 architecture frameworks for image classification," in *2021 International conference on disruptive technologies for multi-disciplinary research and applications (CENTCON)*, vol. 1. IEEE, 2021, pp. 96–99.

[30] C. Lu, Y. Zhou, F. Bao, J. Chen, C. Li, and J. Zhu, "Dpm-solver++: Fast solver for guided sampling of diffusion probabilistic models," *arXiv preprint arXiv:2211.01095*, 2022.

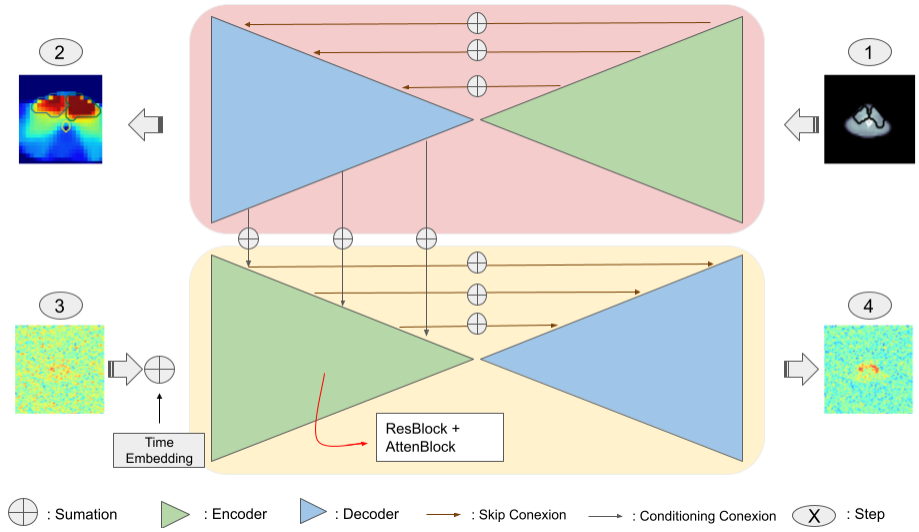

Fig. 1. Image to image Diffusion Probabilistic Model. The model begins with 2D CT scans containing segmented OARs and PTVs (Step 1). The conditioning UNet (red block) then predicts the dosimetry (Step 2). Next, the denoising model (yellow block) sequentially removes noise from the image until the dosimetry is generated (Step 4). At each step, the model learns the amount of noise to remove using the timestamp embedding (Step 3) and the conditioning features (skip conexions between red and yellow blocks).

Target	**Metric**	**Rule 1**	**Rule 2**	**Rule 3**	**Rule 4**	**Rule 5**	**Rule 6**	**Rule 7**	**Rule 8**	**Rule 9**	**Rule 10**
BRAINSTEM	$d_{0.1cc}$		HIGH	LOW	LOW	LOW	LOW	LOW	LOW	LOW	LOW
SPINAL CORD	$d_{0.1cc}$	HIGH		LOW	LOW	LOW	LOW	LOW	LOW	LOW	LOW
PAROTID	d_{mean}			LOW	MEDIUM	HIGH	MEDIUM	MEDIUM	LOW	LOW	HIGH
ESOPHAGUS	d_{mean}			LOW	MEDIUM	LOW	LOW	LOW	LOW	LOW	LOW
	$d_{0.1cc}$			LOW	MEDIUM	LOW	MEDIUM	LOW	LOW	LOW	HIGH
LARYNX	d_{mean}			LOW	MEDIUM	HIGH	LOW	LOW	LOW	LOW	HIGH
	$d_{0.1cc}$			LOW	MEDIUM	HIGH	LOW	HIGH	LOW	HIGH	LOW
MANDIBLE	$d_{0.1cc}$			LOW	HIGH	MEDIUM	LOW	LOW	LOW	MEDIUM	HIGH
PTV50	d_{95}			HIGH	HIGH	HIGH	LOW	LOW	HIGH	HIGH	HIGH
	d_{01}			LOW	HIGH	LOW	MEDIUM	MEDIUM	LOW	LOW	LOW
PTV63	d_{95}			HIGH	HIGH	HIGH	HIGH	LOW	HIGH	HIGH	HIGH
	d_{01}			LOW	HIGH	LOW	MEDIUM	MEDIUM	LOW	MEDIUM	LOW
PTV70	d_{95}			LOW	HIGH	HIGH	HIGH	HIGH	HIGH	HIGH	HIGH
	d_{01}			LOW	HIGH	LOW	MEDIUM	MEDIUM	LOW	LOW	LOW
Treatment type:		BAD	BAD	BAD	ENOUGH	ENOUGH	ENOUGH	ENOUGH	GOOD	GOOD	BAD

TABLE I
THIS TABLE SHOWS THE SET OF FUZZY RULES THAT COMPLETE THE SYSTEM.

Model	**Chaos (ω)**	**DS**	**DVHS**
Balanced			
	0	7.204	5.461
	0.15	8.425	6.56
	0.3	10.306	8.04
Biased			
	0	9.069	11.459
	0.15	9.991	11.662
	0.3	11.684	11.897
Aggressive			
	0	5.302	4.507
	0.15	6.658	5.43
	0.3	8.919	7.02
Conservative			
	0	5.445	4.23
	0.15	6.877	5.518
	0.3	9.138	7.242

TABLE II
DPM RESULTS BASED ON MODEL/CHAOS COMBINATIONS.

Aggregation	**Consequent**	**Train MAE**	**Test MAE**
Eq. 6	Linear	1.504 ± 0.034	1.631 ± 0.096
Eq. 6	Non linear	1.492 ± 0.029	1.580 ± 0.061
Product	Linear	1.806 ± 0.032	1.900 ± 0.091
Product	Non linear	1.711 ± 0.035	1.817 ± 0.027

TABLE III
ANFIS MODEL RESULTS

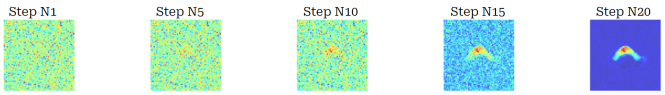

Fig. 2. Performing sampling in 20 steps with DPM Solver ++ and cosine scheduler.

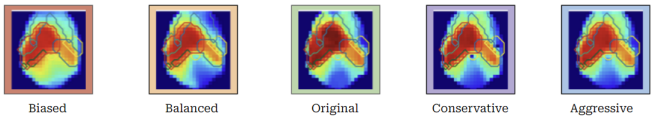

Fig. 3. Differences in predictions between four DPM models for patient 246 within the evaluation data partition.

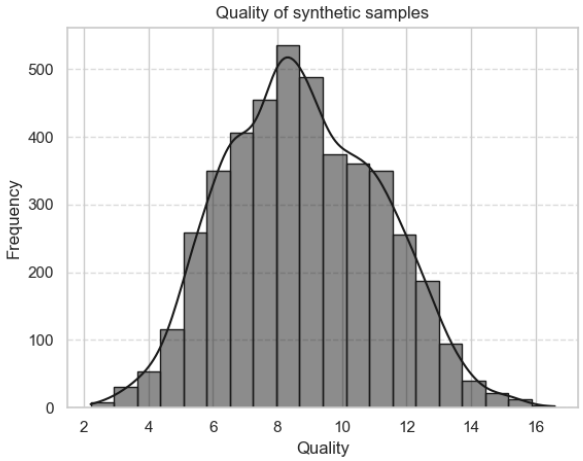

Fig. 4. Distribution of treatment quality obtained by the DPMs. For each diffusion model, 5 treatments are sampled and combined with the CUNet output depending on the chaos parameters set at 0%, 15%, and 30%.

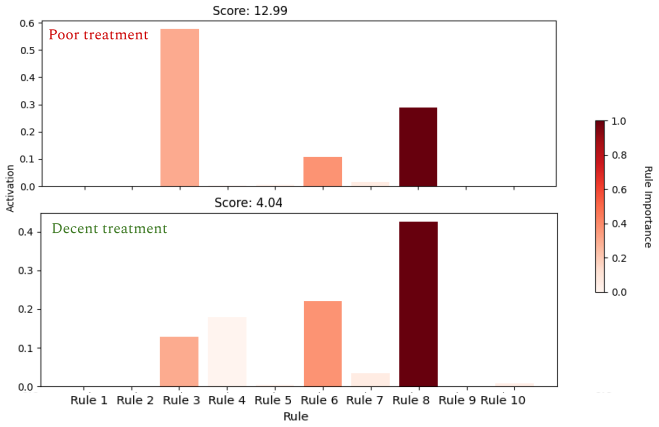

Fig. 5. Illustrative example of a comparison between a bad and a decent treatment. The plot shows the activation of each rule (y-axis) and the colour represents the importance of each rule in the ANFIS.

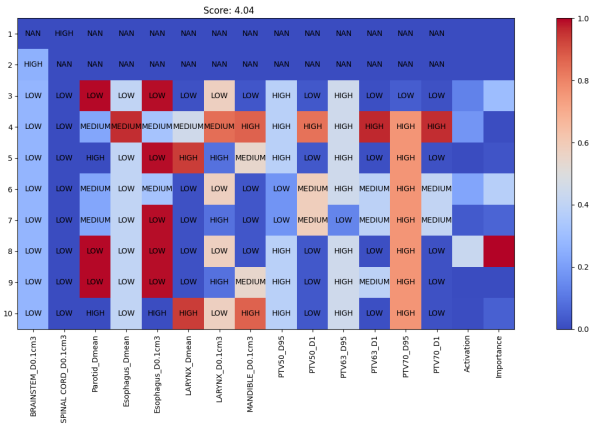

Fig. 6. This figure shows a heat map in which the colour represents the membership of each premise within each rule of the ANFIS.

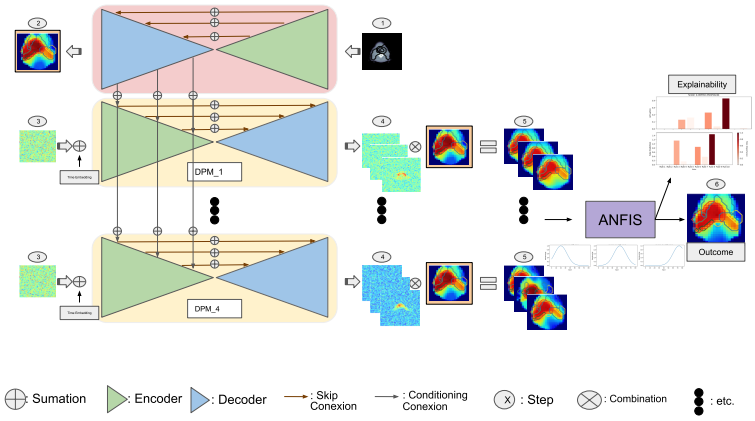

Fig. 7. Experimental KBP framework for IMRT planning.